Research Report R81-3

NASA-CR-169355
19820025649

FINITE ELEMENT MODELING OF NONISOTHERMAL POLYMER FLOWS

by

David Roylance

August 14, 1981

MIT

DEPARTMENT
OF
CIVIL
ENGINEERING

SCHOOL OF ENGINEERING
MASSACHUSETTS INSTITUTE OF TECHNOLOGY
Cambridge, Massachusetts 02139

Finite Element Modeling of Nonisothermal Polymer Flows

David Roylance
Department of Materials Science and Engineering
Massachusetts Institute of Technology
Cambridge, Massachusetts 02139

A manuscript for the ACS Symposium Series
"Computer Applications in Coatings and Plastics"

August 14, 1981

Abstract.

This paper describes a finite element formulation designed to simulate polymer melt flows in which both conductive and convective heat transfer may be important, and illustrates the numerical model by means of computer experiments using extruder drag flow and entry flow as trial problems. Fluid incompressibility is enforced by a penalty treatment of the element pressures, and the thermal convective transport is modeled by conventional Galerkin and optimal upwind treatments.

Introduction

Process development for polymer melt flow operations has in the past been largely empirical, due in part to the difficulty of obtaining closed-form solutions to the governing equations which satisfy the complicated boundary conditions encountered in actual equipment. The finite element method promises a significant advance in our capability to obtain numerical solutions to these processing problems, in that it is able to generate approximate solutions for irregularly shaped boundaries. In an earlier paper (1) this author described the utility of "penalty" finite elements in predicting the velocity and stress fields developed in melt processing, and this paper will describe the extension of this method to include coupled heat transport effects. It is hoped that such a capability will help the process

designer avoid such processing problems as thermomechanical degradation or improperly sized equipment, and further to process materials so as to produce optimal microstructures and properties.

Formulation

The analyses to be reported here were obtained by means of isoparametric penalty elements developed at MIT and incorporated within the finite element analysis program FEAP listed in the text by Zienkiewicz (2). The element formulation will be described briefly here, and the reader new to finite element methodology is referred to standard texts on the subject (2,3) for a more extensive discussion of the various concepts. The description here will be that for plane flow problems, but the concepts are readily extended to axisymmetric and three-dimensional formulations as well.

The solution domain of the problem is discretized as an assemblage of elements along whose boundaries are located nodes at which velocities $\underline{u}_i$ and temperatures T_i are sought. (The i subscript ranges over the element nodes, and underlining indicates a vector or matrix quantity.) The nodal values of the x and y components of velocity and the temperature are listed in a vector $\underline{a}_i$:

$$\underline{a}_i^T = (u_i, v_i, T_i) = (\underline{u}_i, T_i)$$

The values of velocity and temperature at an arbitrary position within an element can be approximated by interpolating among the nodal values:

$$\underline{u}(x,y) = N_i(x,y)\ \underline{u}_i$$
$$T(x,y) = N_i(x,y)\ T_i$$

The interpolation functions $N_i(x,y)$ are obtained from standardized subroutines and can be selected to provide linear, quadratic, or higher-order interpolation among the nodal values. This interpolation is a central concept in finite element analyses, in that the actual variation of the unknowns within an element is replaced by a low-order polynomial interpolation.

The rate-of-deformation tensor $\underline{V}$ can be obtained from the velocity field as:

$$\underline{V}^T = (\partial u/\partial x,\ \partial v/\partial y,\ \partial v/\partial x + \partial u/\partial y)$$

$$\underline{V} = \underline{L}\underline{u} = \underline{L}N_i\underline{u}_i = \underline{B}_i\underline{u}_i$$

$$\underline{L} = \begin{bmatrix} \partial/\partial x & 0 \\ 0 & \partial/\partial y \\ \partial/\partial y & \partial/\partial x \end{bmatrix} \qquad \underline{B}_i = \begin{bmatrix} N_{i,x} & 0 \\ 0 & N_{i,y} \\ N_{i,y} & N_{i,x} \end{bmatrix}.$$

In the case of Newtonian fluids of viscosity μ, the deviatoric stresses $\underline{\tau}$ can be obtained from $\underline{V}$ as:

$$\underline{\tau}^T = (\tau_{xx}, \tau_{yy}, \tau_{xy})$$

$$\underline{\tau} = \underline{D}\ \underline{V}$$

$$\underline{D} = \mu \begin{bmatrix} 2 & 0 & 0 \\ 0 & 2 & 0 \\ 0 & 0 & 1 \end{bmatrix}$$

The hydrostatic stress p can be obtained by considering the volumetric dilation V_v:

$$V_v = \nabla^T \underline{u} = \underline{m}^T \underline{B}_i \underline{u}_i$$

$$\nabla^T = (\partial/\partial x,\ \partial/\partial y), \quad \underline{m}^T = (1,1,0)$$

$$p = \lambda V_v = \lambda \underline{m}^T \underline{B}_i \underline{u}_i$$

Here λ is comparable to the fluid bulk modulus, and in the case of incompressible fluids can be regarded as a parameter which "penalizes" fluid compressibility. By appropriate choice of λ (generally λ is chosen as $10^7 \mu$ (4)), incompressibility can be enforced to whatever degree is desired. The total stress $\underline{\sigma}$ is then:

$$\underline{\sigma} = \underline{\tau} + \underline{m}p$$

The nodal unknowns $\underline{a}_i$ are to be chosen so as to satisfy

the governing equations in an integral sense; this can be done by using a Galerkin weighted residual formulation of the conservation equations for momentum and energy transport:

$$\int N_i (\underline{L}^T \underline{\sigma}) \, d\Omega = 0$$

$$\int N_i (\nabla^T k \nabla T + Q) \, d\Omega = 0$$

Here Ω is the element area, Q is the internal heat generation, k is the thermal conductivity, and the weighting functions N_i are the same functions used for interpolation. Using Green's theorem on the above integrals and substituting the interpolated expressions for $\underline{\sigma}$ and T, one obtains the matrix equation:

$$\underline{Ka} = \underline{f}$$

where

$$K = \begin{bmatrix} K^\lambda + K^\mu & 0 \\ 0 & K^T \end{bmatrix} \qquad f = \begin{Bmatrix} f^u \\ f^T \end{Bmatrix}$$

$$K^\lambda_{jk} = \int (\underline{m}^T \underline{B}_j)^T \lambda (\underline{m}^T \underline{B}) \, d\Omega$$

$$K^u_{jk} = \int \underline{B}_j^T \underline{\underline{D}} \underline{B}_k \, d\Omega$$

$$K^T_{jk} = \int (\nabla^T N_j) k \nabla N_k \, d\Omega$$

$$f^u = \int N_i \underline{t}^* \, d\Gamma$$

$$f^T = \int N_i Q \, d\Omega$$

The jk subscripts identify the influence of the velocity (or temperature) of the kth node on the force (or thermal flux) at the jth node, and the $\underline{t}^*$ refers to tractions applied to the element boundary Γ. In these analyses Q is taken as arising only from viscous dissipation:

$$Q = \underline{\tau}^T \underline{V}$$

The FEAP code is configured to cycle through each element in turn, evaluating the various K's and f's by Gauss-Legendre numerical integration and adding each element's stiffness or loading to the global arrays relating all of the problem's nodal unknowns (the a's) to the loading terms (the f's). In the analyses to be presented below, four-node linear or eight-node parabolic quadrilateral elements were used in conjunction with 2x2 numerical integration on the K^u and K^T terms. "Selective reduced integration" was used to evaluate the K^λ terms; this reduced integration order is necessary to prevent the large λ parameter from driving the $\underline{a}$ vector to zero (2,4).

Iteration must be used if the coefficients in the formu-

lation (the μ, k, Q) depend on the final solution for $\underline{a}$. In the solutions to be given below, the μ and k are taken as constant, and the velocity and temperature fields are coupled only through the Q term. Here only two iterations are necessary: the velocities and viscous dissipation are computed correctly in the first iteration, and the thermal values in the second.

Although momentum convection is generally negligible for polymer melt flows (Reynolds' numbers on the order of 10^{-5}), thermal convection may be significant. The ratio of convective to conductive transport is given approximately by the Peclet number Pe:

$$Pe = Uh\rho c_p/k.$$

Here U and h are a characteristic velocity and length, while ρ and c_p are the fluid density and specific heat. Using typical values for down-channel extruder drag flow of low density polyethylene (5), for instance, one computes Pe $\simeq$ 5000.

Thermal convection can be incorporated in the finite element analysis by adding to the K^T terms the quantity

$$K^c_{jk} = \int N_j \rho c_p \underline{u}^T \nabla N_k \, d\Omega$$

Incorporation of this term is straightforward, since the velocities $\underline{u}$ are known after the first iteration. The con-

vective terms are unsymmetric, however, which requires using less efficient storage and solution schemes than are possible for symmetric systems. Even more seriously, inclusion of convective transport effects tends to produce numerical instability in the computed results, as will be illustrated below.

Down-channel extruder flow.

The capabilities of the coupled flow-heat transfer model will be illustrated first by means of a simulation of down-channel extruder flow, which may be modeled by the usual unwound-channel approximation as a straight rectangular channel containing fluid which is being dragged downstream by a plate covering the channel top (1,5). This is the well-known Couette flow problem, and is useful as a model problem both by virtue of its relevance to extruder flow and by the availability of theoretical solutions against which the numerical results may be checked. Figure 1 shows the normalized velocity and temperature distributions across the channel height, where the drawn curves are the theoretical predictions and the open symbols are the numerical values obtained using a 4x4 mesh of eight-noded parabolic elements. The theoretical temperature variation is given as

$$T^* = (Br/2)y^* (1-y^*)$$

Here y^* is the height from the root of the channel normalized on the total channel height, $T^* = (T-T_w)/T_w$ is the temperature relative to the wall temperature, and $Br = \mu V^2/k$ is a Brinkman number which provides an indicator of the importance of viscous dissipation relative to heat conduction. The numerical results of figure 1 were obtained with Br = 8.

Figure 2 displays the results of a simulation of a slightly more complicated extension of the problem of figure 1. Here the root and barrel temperatures are different, and the flow is retarded by the presence of a pressure gradient which is positive in the downstream direction. This simulation is more typical of extruder operation, in which the barrel but not the screw is heated and the constriction at the die produces a pressure gradient.

Entry flow.

Entry flow is a much-studied problem which provides a more demanding test of numerical codes than does the viscometric Couette flow problem described above. Theoretical and numerical aspects of this flow have been reviewed recently by Boger (6), and comparison with these other results provide a check of at least the flow aspects of the model. A reservior-to-capillary size ratio of 4:1 was selected, since the flow results become independent of size ratio at this value or larger. Figure 3 shows the grid of 100 four-node

linear elements used to model the upper symmetric half of this problem (273 degrees of freedom), and the portion of the velocity field near the throat. A fully-developed Poiseuille velocity distribution was imposed on the entrance to the reservoir. The velocity distribution in the capillary becomes stable within a few diameters of the entrance, but the field is perturbed far upstream. Figure 4 shows the streamlines developed from the flow field by contour integration along vertical lines through the grid, and normalized so as to be zero along the boundaries and unity along the centerline. These streamlines are identical with published experimental and numerical results, although the grid used here was not intended to be fine enough to capture the weak recirculation which develops in the stagnant corner of the reservoir.

Figure 5 shows the contours of shear stress near the throat, normalized on the theoretical value expected at the capillary wall. The shear contours are in agreement with the isochromatic fringes seen in birefringence photography of entry flow (7), which is an example of a possible experimental verification of the flow model.

Although certain grids using the penalty formulation are known to develop a pathology known as "checkerboarding" in which the computed pressures oscillate from element to element (4), this grid is free of that troublesome (but fixable) result. Figure 6 shows the profile of computed pressures along the elements adjacent to the centerline,

normalized on the value expected in the reservoir in the absence of entry or exit pressure losses. As is well known, the development of the flow field at the entrance to the capillary produces an additional pressure drop which must be accounted for in capillary viscometry by means of a "capillary correction factor". The correction factor, defined as he entrance pressure drop ΔP_{ent} divided by twice the capillary wall shear stress, is given by Boger as 0.589 based on the numerical and experimental work of several workers. The value computed from the data of figure 6 is 0.594, which is within 1% of Boger's value.

As described above, the temperature field is computed using the finite element formulation of the heat conduction equation, with the viscous heat generation being computed from the stress and velocity fields obtained during the first iteration of the problem. The temperature contours, normalized on the maximum centerline temperature $T_c = \mu V^2/3k$ expected for capillary Poiseuille flow, are shown in figure 7. A hot spot is noted just upstream of the entrance, due to the combination of increased dissipation and greater distance from the cooler boundaries at this position. This hot spot leads to higher temperatures both upstream and downstream than would have been expected in simple Poiseuille flow, due to conductive heat transfer from the hot region.

The temperature map of figure 7 is for Pe = 0, the case for which convective terms are not included in the heat transport calculations. Whereas all convective terms vanish

identically in the Couette flow described in the previous section, convective terms are present in the entry flow problem, and these might be expected to be significant for many real problems in the flow of polymer melts through dies. Figure 8 shows the profile of temperatures along the centerline for several values of Peclet number (Pe based on the capillary half-height and the maximum velocity). It is seen that increasing convective transport serves to carry the cooler upstream particles downstream so as to diminish both the magnitude of the hot spot and its ability to conduct heat upstream. As Pe increases, the influence of the entrance region is compressed into a smaller and smaller boundary layer at the throat, leading to numerical difficulties associated with the inability of the fixed mesh to capture effects which occur in the smaller region. At Pe = 10, the values computed by the conventional Galerkin process (solid lines) suffer from noticeable instability, and by Pe = 100 the Galerkin solution has degenerated completely to meaningless values.

The instability associated with convection analyses has plagued both finite difference and finite element analyses, and in recent years several ad hoc treatments have been proposed for obtaining stable and nonoscillatory results in the presence of strong convective terms. One of the most popular of these treatments is "upwinding", in which the upstream portion of the interpolation is weighted more heavily in an attempt to smooth out the high local downstream

gradients which cause the problem in convective flows. The dotted lines in figure 8 were obtained using a convenient "optimal" upwinding formulation suggested by Hughes (4), in which the upwind weighting is obtained simply by relocating the integration point at which the element shape functions are evaluated. The position of the upwind point is determined for each element based on its local Peclet number, so that optimum results may be obtained. Figure 8 shows that the upwind solution for Pe = 10 is considerably smoother than the Galerkin result, and that the results for Pe = 100 in which the upstream temperatures are carried well into the capillary are captured in a smooth and reasonable manner. The reader is cautioned, however, that the use of these upwinding procedures is still controversial, and is directed to a provocative paper by Gresho and Lee (8) in which the drawbacks of this approach are detailed.

Conclusion.

This paper has described an analytical tool which can predict velocities, stresses, and temperatures in nonisothermal flow situations of the sort encountered in many polymer melt processing operations. Such a model cannot be expected to replace the experience and intuition which provide the basis for most process design today, but it is hoped that this inexpensive and easily implemented model can provide a means by which the process designer's intuition

might be expanded. Properly used, it can be a valuable additional tool at the process designer's disposal.

Development of this model is continuing in our laboratory, and among the aspects still under development are capabilities for transient flows, reactive fluids, free surfaces, and wall slip. Although incorporation of fluid elasticity is desired due to its importance in many polymer melt flows, such a development has proven elusive to a number of well qualified groups in the past several years. At present, it seems prudent to let the theoretical aspects of elastic effects be developed further before attempting their incorporation in a general process model.

Acknowledgements.

The author gratefully acknowledges the support of this work by the Army Materials and Mechanics Research Center, and by the National Aeronautics and Space Administration through MIT's Materials Processing Center.

Literature Cited.

1. Roylance, D. Polym. Eng. Sci. 1980, 20, 1029-34.
2. Zienkiewicz, O.C. "The Finite Element Method"; McGraw-Hill: London, 1977.
3. Segerlind, L.J. "Applied Finite Element Analysis"; John Wiley: New York, 1976.
4. Hughes, T.R.J.; Liu, W.K.; Brooks, A. J. Comp. Physics

1979, 30, 1-60.

5. Tadmor, Z.; Klein, I. "Engineering Principles of Plasticating Extrusion"; Van Nostrand Reinhold: New York, 1970.
6. Boger, D.V. "Circular Entry Flows of Inelastic and Viscoelastic Fluids"; to appear in "Advances in Transport Processes"; Wiley International.
7. Han. P. "Rheology in Polymer Processing"; Academic Press: New York, 1976; 98-105.
8. Gresho, P.M.; Lee, R.L. Computers and Fluids 1981, 9, 223-253.

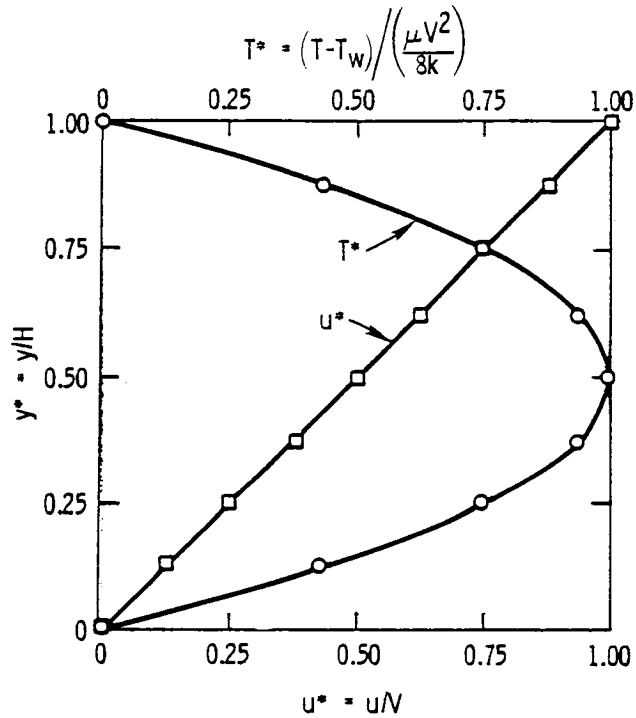

Figure 1 - Normalized velocity and temperature distributions in Couette flow.

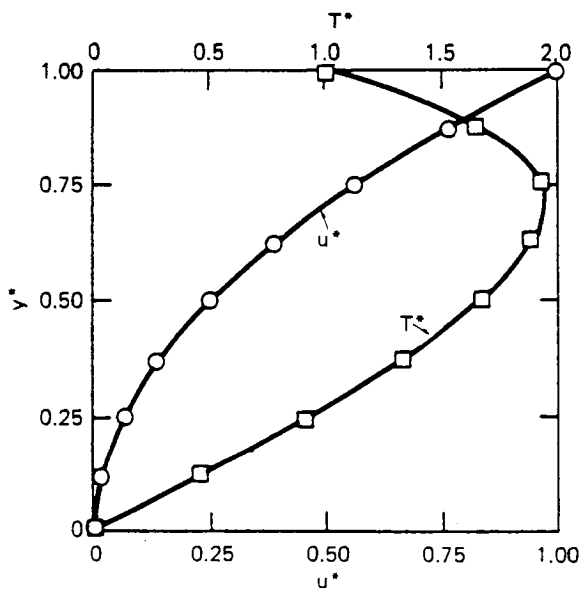

Figure 2 - Couette flow with imposed pressure gradient, and with different root and barrel temperatures.

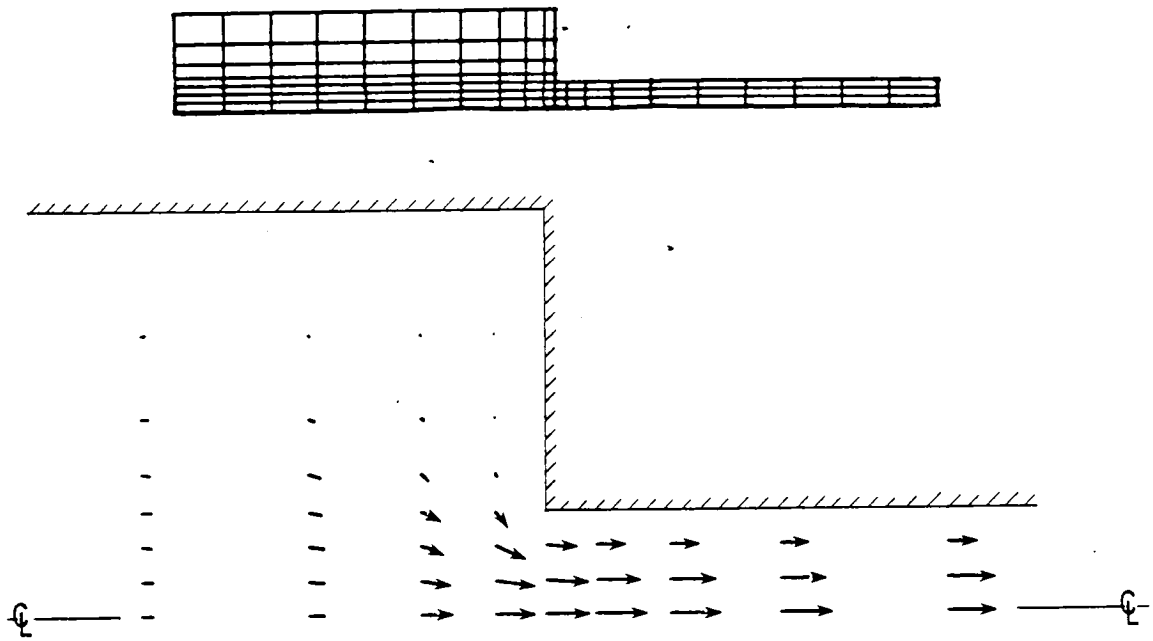

Figure 3 -Finite element mesh and computed velocity field for 4:1 entry flow.

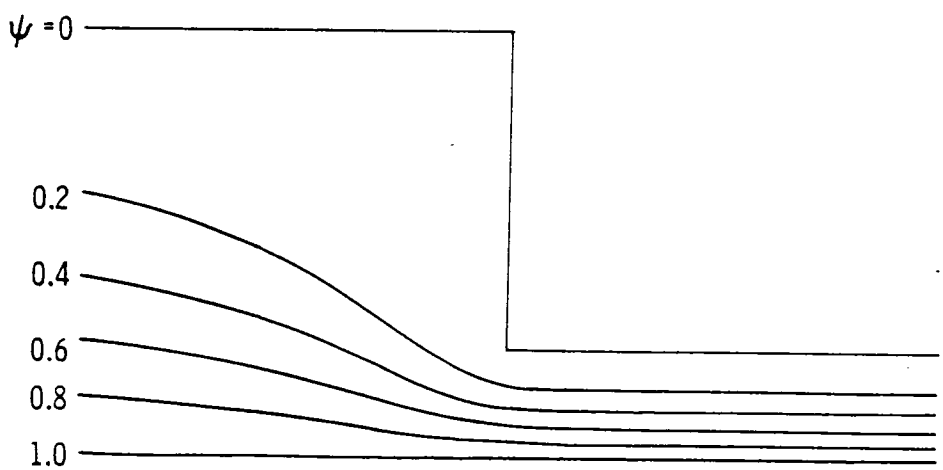

Figure 4 - Entry flow streamlines.

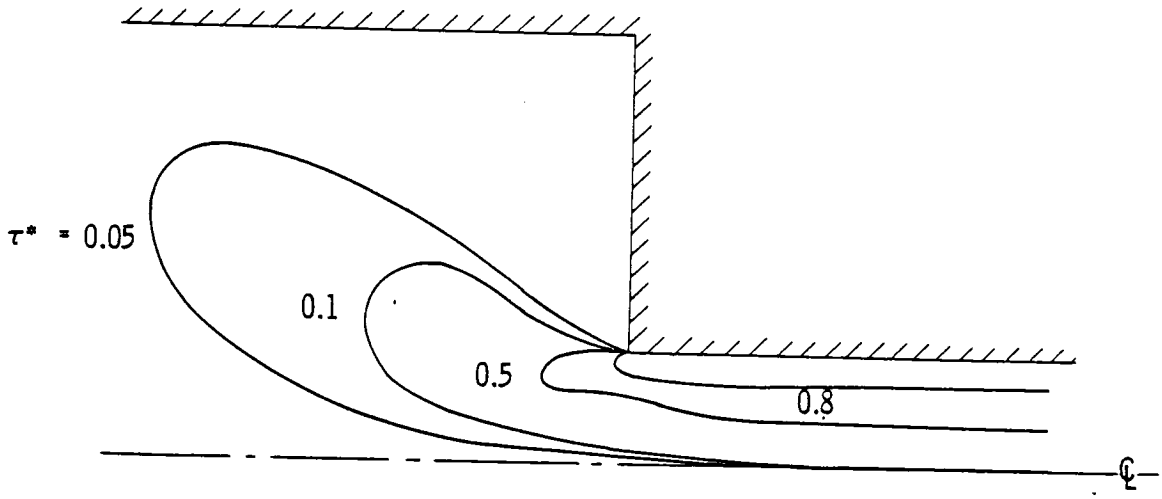

Figure 5 - Shear stress contours for 4:1 entry flow.

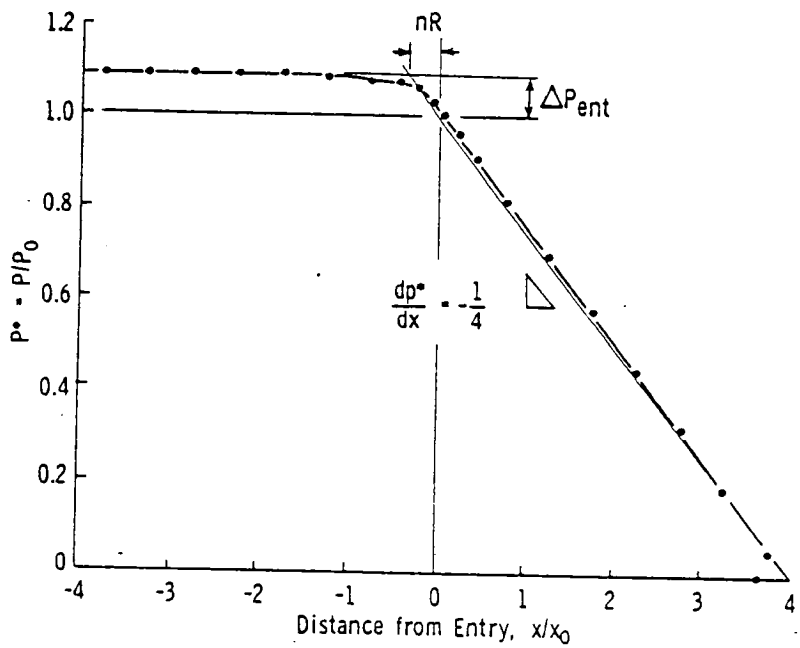

Figure 6 -Normalized pressures along centerline.

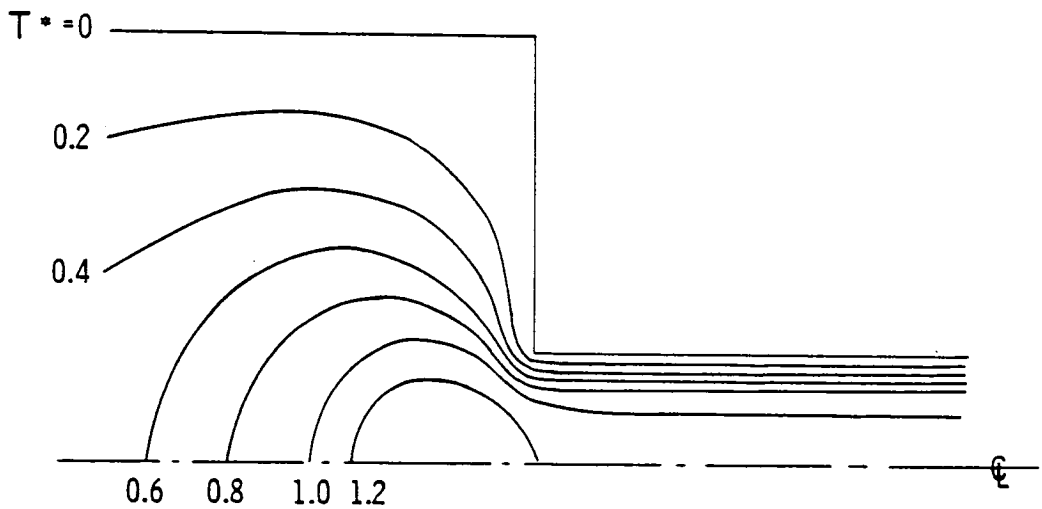

Figure 7 - Temperature contours for 4:1 entry flow, Pe = 0.

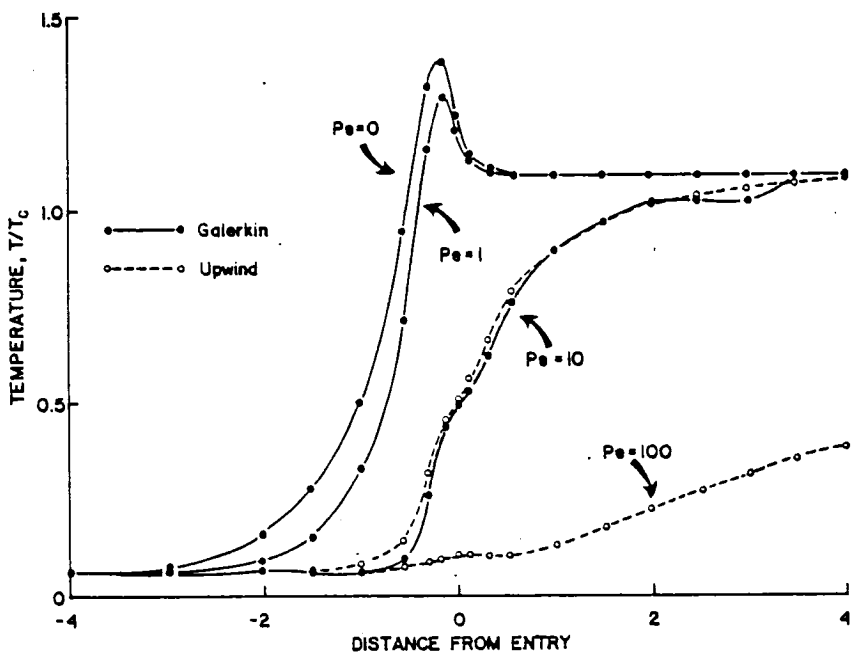

Figure 8 - Centerline temperatures at various Peclet numbers.